Available online at www.sciencedirect.com

ScienceDirect

Procedia Structural Integrity 23 (2019) 571–576

Structural Integrity Procedia

www.elsevier.com/locate/procedia

9th International Conference on Materials Structure and Micromechanics of Fracture

Crack tip mechanisms: a numerical analysis

F.V. Antunes[a], M.F. Borges[a], B. Marques[a], P. Prates[a], R. Branco[a]*

[a] CEEMPRE, University of Coimbra, Rua Luís Reis Santos, 3030-788 Coimbra, Portugal

Abstract

Fatigue crack propagation is usually studied using da/dN-ΔK curves obtained experimentally. However, the use of ΔK does not provide any information into the mechanics which occur at the crack tip and are effectively responsible for fatigue crack growth. The objective here is to study crack tip phenomena using the CTOD. The aspects studied are the crack closure level, the elastic regime of ΔK and the crack tip plastic deformation, which was related with fatigue crack propagation. The elastic load range, ΔK_{el}, was found to increase linearly with material's yield stress. Well defined relations were found between the elastic and the plastic deformations, which greatly depend on material. The fatigue crack growth rate, obtained experimentally, was plotted versus plastic CTOD range, δ_p, for the different materials. Finally, the CTOD versus load curves were used to predict fatigue threshold and to study material hardening after crack propagation.

Keywords: Fatigue crack propagation; CTOD; crack closure; fatigue threshold.

1. Introduction

Fatigue crack propagation is usually studied using da/dN-ΔK curves obtained experimentally. K is an elastic parameter, which quantifies the strength of stress singularity at the crack tip, assuming a linear elastic behavior for the material. The approach based on ΔK has several advantages, namely: (i) Many solutions of K already exist in literature for different cracked geometries; (ii) The numerical determination of K is relatively simple using commercial FEM software; (iii) K can also be determined experimentally, using Digital Image Correlation

* Corresponding author. Tel.: 00351-934798913; fax: 00351-239790701.
E-mail address: fernando.ventura@dem.uc.pt

10.1016/j.prostr.2020.01.147

technique, for example; (iv) There is a linear region of da/dN-ΔK in log-log scales, named Paris law regime, which is widely used in design; (v) The expression includes the effect of crack length and load; (vi) The major part of fatigue crack growth (FCG) studies have been developed using da/dN-ΔK curves, therefore there are many results for comparison; (vii) The researchers devoted to experimental analysis can develop independent work, without the need of a parallel numerical analysis. However, the use of ΔK does not provide any information into the mechanics which occur at the crack tip and are effectively responsible for fatigue crack growth.

Experimental techniques have been used to observe crack tip phenomena, namely Scanning Electronic Microscopy (SEM), Digital Image Correlation (DIC) or tomography. DIC is now being widely used to analyze crack tip fields at the surface of the material (Mokhtarishirazabad, 2016). SEM have been used to observe fatigue crack propagation in-situ (Yan and Fan, 2016; Zhang and Liu, 2012). The analysis inside the specimen, which is more difficult, is made using synchrotron X-ray diffraction (Lopez-Crespo et al., 2015).

The numerical studies can also be used to analyze stress and strain fields around crack tip. In fact, numerical models based on the finite element method permit an insight into the basic mechanisms responsible for FCG. They can be used to study 3D crack fronts, which is not easy experimentally because only the surface of the specimen is available for direct measurements. The numerical approaches are also particularly adequate to develop parametric studies focused on the effect of loading, geometry or material parameters. The objective in this study is study crack tip phenomena using numerical values of crack tip opening displacement (CTOD).

Nomenclature

a	Crack length
CTOD	Crack tip Opening Displacement
C_X	Kinematic saturation coefficient
C_Y	Isotropic saturation coefficient
DIC	Digital Image Correlation
K	stress intensity factor
SEM	Scanning Electronic Microscopy
W	Specimen´s width
X_{sat}	kinematic saturation stress
Y_{sat}	Isotropic saturation stress
Y_0	Yield Stress
Δa	Crack propagation
ΔK	Range of stress intensity factor

2. Numerical model

Figure 1 presents the geometry of the specimens considered in this study. M(T) and CT specimens with different sizes were studied, as indicated in Table 1. Sharp cracks were assumed with different initial lengths. Only 1/8 of M(T) specimen and ¼ of CT specimens were modeled considering adequate boundary conditions, as indicated in Figure 1. Pure plane strain state was simulated restraining out-of-plane deformation, as illustrated in Figure 1c. In some special cases the contact of crack flanks was removed numerically, and this is identified along the paper by the expression “no contact”. The quality of material modeling is fundamental for the accuracy of numerical predictions. The elastic-plastic models adopted in this work assume: (i) the isotropic elastic behaviour modeled by the generalised Hooke’s law; (ii) the plastic behavior following the von Mises yield criterion, coupled with Voce isotropic hardening law (Voce, 1948) and Armstrong-Frederick non-linear kinematic hardening law (Chaboche, 2008), under an associated flow rule. Table 2 presents the constants assumed for the different materials. All finite element meshes comprised two main regions: an ultra-refined rectangular box, near the crack tip, created with elements of 8×8 μm side; and a coarser mesh in the remaining volume of the body in order to reduce the computational overhead. In the thickness direction, only one layer of elements was used. The crack propagated uniformly over the thickness, at the minimum load, by successive debonding of both crack front nodes. A total of

159 crack propagations were modeled, corresponding to a crack advance (Δa) of 1272 μm (i.e., Δa = (160-1)×8 μm). Between each crack increment, which corresponds to one finite element, were applied five load cycles. The numerical model was implemented in the DD3IMP in-house code (Oliveira et al., 2008). This implicit finite element software, originally developed to model deep drawing, uses three-dimensional elements. The evolution of the deformation process is described by an updated Lagrangian scheme, assuming a hypoelastic-plastic model. Thus, the mechanical model takes into account large elastoplastic strains and rotations and assumes that the elastic strains are negligibly small with respect to unity. The contact of the crack flanks is modeled considering a rigid body (plane surface) aligned with the crack symmetry plane. A master–slave algorithm is adopted and the contact problem is treated using an augmented Lagrangian approach.

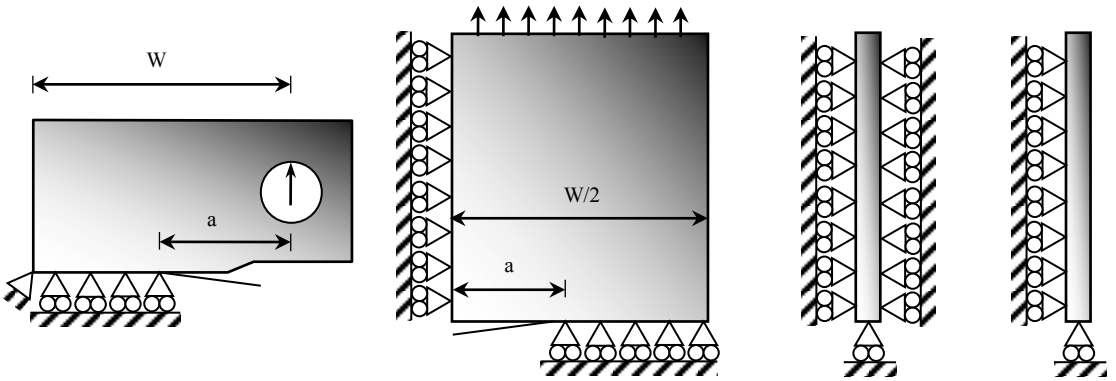

Fig. 1. Models of (a) C(T) specimen; (b) M(T) specimen. (c) Plane strain state. (d) Plane stress state.

Table 1. Elastic-plastic parameters for the materials under study (AA- Aluminium Alloy; SS – Stainless Steel).

			Hooke's law parameters		Isotropic hardening (Voce)			Kinematic hardening (Armstrong-Frederick)	
Material		W [mm]	E [GPa]	ν [-]	Y_0 [MPa]	Y_{Sat} [MPa]	C_Y [-]	C_X [-]	X_{Sat} [MPa]
AA6082-T6 (Antunes et al., 2016)	MT	60	70	0.29	238.15	487.52	0.01	244.44	83.18
AA7050-T6 (Antunes et al., 2017)	MT	50	71.7	0.33	420.50	420.50	0	228.91	198.35
AA2050-T8 (Antunes et al., 2018)	MT	50	77.4	0.30	383.85	383.85	0	97.38	265.41
AA6016-T4	MT	60	70	0.29	124.00	415.00	9.5	146.50	34.90
304L SS	CT	50	196	0.3	117	87	9	300	176
18Ni300 steel	CT	36	160	0.30	683.62	683.62	0	728.34	402.06

3. Results

Figure 2 presents a typical variation of CTOD with load, predicted numerically. The CTOD was measured at the first node behind crack tip, at a distance of 8 μm, because this is the most sensitive point to crack tip phenomena. The load is presented in the form of σ/Y_0, being σ the remote stress and Y_0 the material's yield stress. Similar plots were obtained experimentally using Digital Image Correlation (Vasco-Olmo et al., 2019), and numerically (Matos and Nowell, 2007; Pommier and Risbet, 2005). The crack is closed for relatively low loads, i.e., between the minimum load (point *A*) and the crack opening load (point *B*). The increase of load above point *B* opens progressively the crack, and the variation of CTOD is linear up to point *C*, where plastic deformation starts. The load range between points *B* and *C* is not expected to contribute to FCG, therefore the effective load range is the difference between the maximum load and the transition between the elastic and the elastic-plastic regimes defined by point *C*. The plastic deformation starts increases progressively up to point *D*. δ_e and δ_p define the elastic and plastic ranges, respectively. The elastic regime during unloading (between points *D* and *E*) has the some slope of the *BC* region, as could be expected. Reversed plastic deformation occurs between *E* and *F*, and crack closure occurs at point *F*.

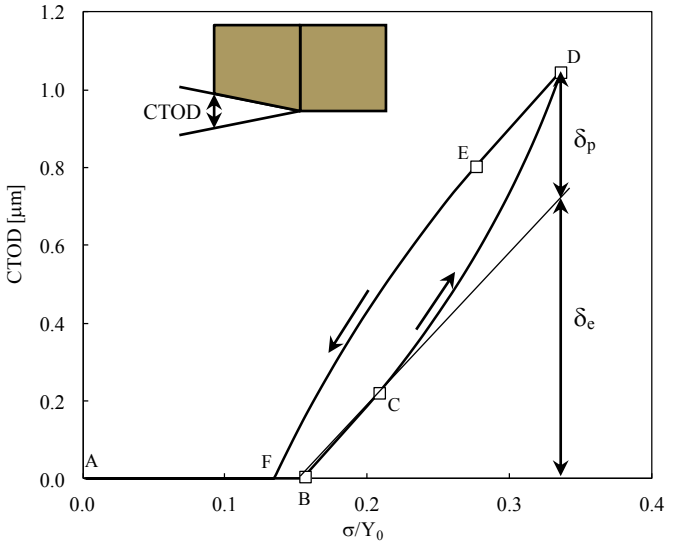

Fig. 2. Typical results of CTOD versus load. (M(T) specimen; plane stress; 6082-T6; F_{min}=0 N; F_{max}=240 N; a=6.272 mm; W=60 mm).

3.1. Crack closure

The CTOD plots can be used to study different aspects of crack closure phenomenon. Figure 3 shows the relation between crack opening and crack closure levels. The crack opening level is higher than the crack closure level and a value of 0.9 was obtained for the ratio between both parameters. It is interesting to notice that the opposite trend is obtained experimentally, i.e., the crack opening level is smaller than the crack closure level.

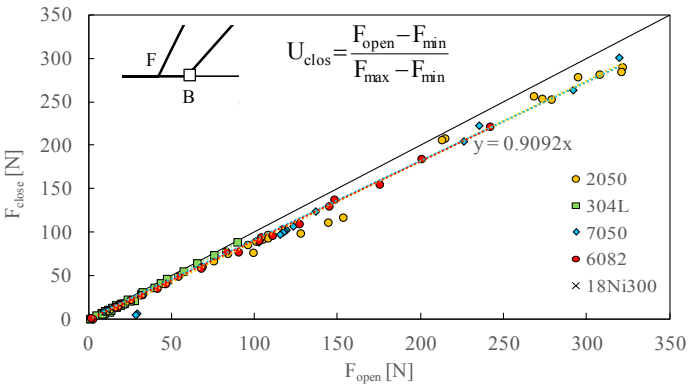

Fig. 3. Crack opening level versus crack closure level.

3.2. Elastic regime

The region between points *B* and *C* in Figure 2 defines the elastic regime, which is not expected to contribute to fatigue crack growth (FCG). Therefore, the effective load range is F_{max}-F_C, being F_C the load corresponding to point *C*, and from this it is possible to obtain the elastic range of ΔK, ΔK_{el}. Figure 4 presents the effect of load range on elastic ΔK for three aluminium alloys (AA) and the 304L stainless steel (SS). The increase of load range produces a linear decrease of ΔK_{el} in the three aluminium alloys. The AA 6082-T6 has values of 2.4 and 1.3 MPa.m$^{0.5}$ for ΔK values of 2.5 and 23.9 MPa.m$^{0.5}$, respectively. On the other hand, in the 304L SS the increase of ΔK increases ΔK_{el}. The scatter of ΔK_{el} in Figure 4 may be explained by the effect of the other loading parameters, namely stress ratio, and by some uncertainty introduced by the numerical procedure. The differences between the alloys are mainly

explained by the initial yield stress. Figure 5 presents the variation of ΔK_{el} with Y_0. The increase of Y_0 increases ΔK_{el}, which is logical since the limit of elastic deformation is defined by the yield stress. The reduction of ΔK_{eff} (by ΔK_{el}) moves the da/dN-ΔK_{eff} to the left side.

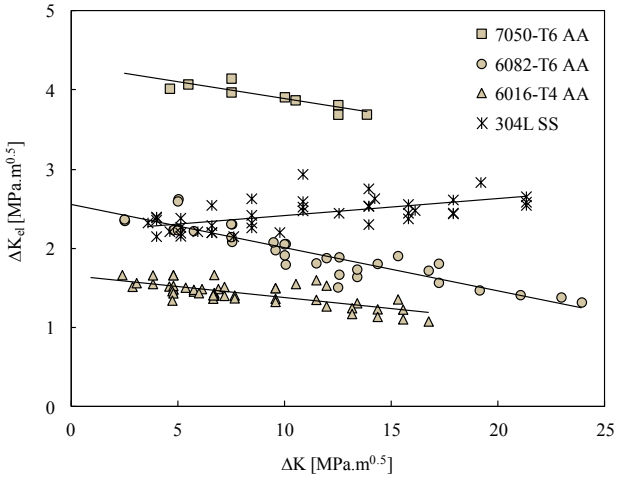

Fig. 4. Effect of load range on ΔKelas (plane stress).

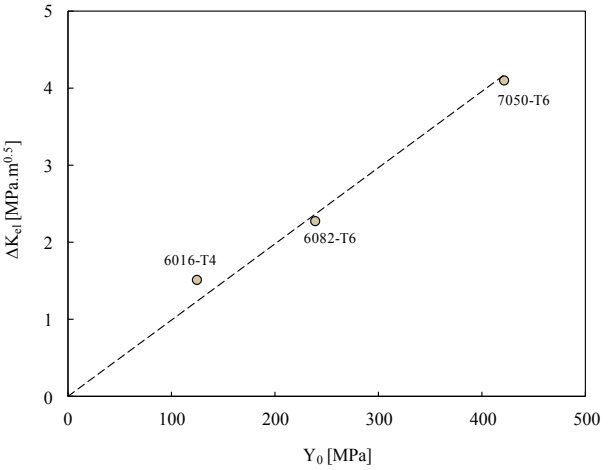

Fig. 5. Effect of yield stress on ΔK_{elas} (plane stress).

3.3. Elastic-plastic regime

Figure 6 shows the variation of plastic CTOD range, δ_p with the elastic deformation range, δ_e. There is a well-defined relation between δ_p and δ_e, which is non-linear. However, there is a great influence of material, and a relatively influence of stress ratio (R) on this relation.

Figure 7 plots the fatigue crack growth rate, da/dN, versus plastic CTOD obtained for different materials. For each material, the increase of δ_p increases da/dN, as is logical since FCG is expected to be linked with crack tip plastic deformation. There is a great difference between materials, which means that for the same plastic deformation at the crack tip there are different fatigue crack growth rates. These da/dN-δ_p relations are expected to be material properties which can be used to predict FCGR for other loading conditions.

The CTOD versus load curve can also be used to predict fatigue threshold.

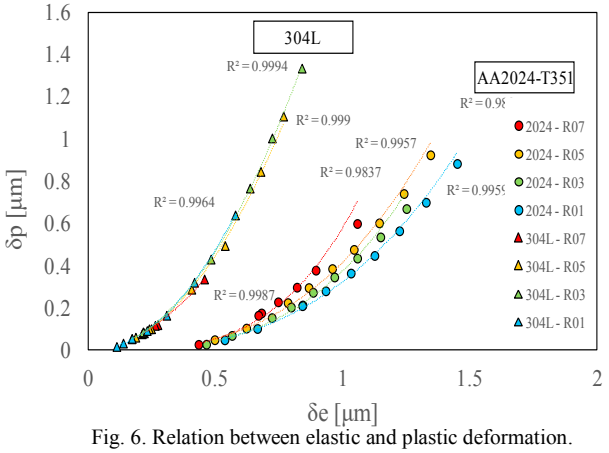

Fig. 6. Relation between elastic and plastic deformation.

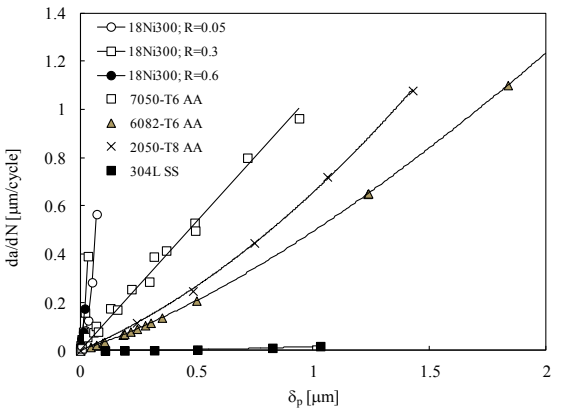

Fig. 7. da/dN versus plastic CTOD range, δ_p.

4. Conclusions

Crack tip phenomena is studied here using CTOD versus load plots obtained numerically. The aspects studied are the crack closure level, the elastic regime of ΔK and the crack tip plastic deformation, which was related with fatigue crack propagation. The elastic load range, ΔK_{el}, was found to increase linearly with material's yield stress. Well defined relations were found between the elastic and the plastic deformations, which greatly depend on material. The fatigue crack growth rate, obtained experimentally, was plotted versus plastic CTOD range, δ_p, for the different materials.

Acknowledgements

This work was financially supported by: Project PTDC/CTM-CTM/29101/2017 – POCI-01-0145-FEDER-029101 funded by FEDER funds through COMPETE2020 - Programa Operacional Competitividade e Internacionalização (POCI) and by national funds (PIDDAC) through FCT/MCTES.

References

Antunes, F.V., Rodrigues, S.M., Branco, R., Camas, D., 2016. A numerical analysis of CTOD in constant amplitude fatigue crack growth, Theoretical and Applied Fracture Mechanics 85, 45–55.

Antunes, F.V., Branco, R., Prates, P.A., Borrego, L., 2017. Fatigue crack growth modelling based on CTOD for the 7050-T6 alloy, Fatigue Fract Engng Mater Struct 40, 1309–1320.

Antunes, F.V., Serrano, S., Branco, R., Prates, P., Lorenzino, P., 2018. Fatigue crack growth in the 2050-T8 aluminium alloy, International journal of fatigue 115, 79–88.

Chaboche, J.L., 2008. A review of some plasticity and viscoplasticity constitutive theories. International Journal of Plasticity 24, 1642–1693.

Yusof F., Lopez-Crespo P., Withers P.J., 2013. Effect of overload on crack closure in thick and thin specimens via digital image correlation. International Journal of Fatigue 56, 17–24.

Lopez-Crespo, P., Steuwer, A. Buslaps, T., Tai, Y.H., Lopez-Moreno, A., Yates, J.R., Withers, P.J., 2015. Measuring overload effects during fatigue crack growth in bainitic steel by synchrotron X-ray diffraction, International Journal of Fatigue 71, 11–16.

Matos, P.F.P., Nowell, D., 2007. On the accurate assessment of crack opening and closing stresses in plasticity-induced fatigue crack closure problems. Engineering Fracture Mechanics 74, 1579–1601.

Mokhtarishirazabad, M., Lopez-Crespo P., Moreno, B., Lopez-Moreno, A., Zanganeh, M., 2016. Evaluation of crack-tip fields from DIC data: A parametric study, International Journal of Fatigue 89, 11–19.

Oliveira, M.C., Alves, J.L. Menezes, L.F., 2008. Algorithms and Strategies for Treatment of Large Deformation Frictional Contact in the Numerical Simulation of Deep Drawing Process. Archives of Computational Methods in Engineering 15, 113-162.

Pommier, S., Risbet, M., 2005. Time derivative equations for mode I fatigue crack growth in metals, International Journal of Fatigue 27, 1297–1306.

Santos, L.M.S., Ferreira, J.A.M., Jesus, J.S., Costa, J.M., Capela, C., 2016. Fatigue behaviour of selective laser melting steel components, Theoretical and Applied Fracture Mechanics 85, 9-15.

Sunder, R., 2012Unraveling the Science of Variable Amplitude Fatigue, Journal of ASTM International 9(1), 1-32.

Vasco-Olmo, J.M., Díaz, F.A., Antunes, F.V., James M.N., 2019. Characterisation of fatigue crack growth using digital image correlation measurements of plastic CTOD, Theoretical and Applied Fracture Mechanics 101, 332–341.

Voce, E., 1948. The relationship between stress and strain for homogeneous deformation. Journal of the Institute of Metals 74, 537–562.

Yan, L., Fan, J., 2016. In-situ SEM study of fatigue crack initiation and propagation behavior in2524 aluminum alloy, Materials and Design, 110, 592-601.

Zhang, W., Liu, Y., 2012. Investigation of incremental fatigue crack growth mechanisms using in situ SEM testing, International Journal of Fatigue 42, 14–23.